A Tandem Momentum Trap for Dynamic Specimen Recovery During Split Hopkinson Pressure Bar Testing of Cancellous Bone

Marianne Prot[1] · **Trevor John Cloete**[2]

Abstract A novel method for dynamic specimen recovery using tandem momentum traps on an otherwise standard split Hopkinson pressure bar, is presented. The method is based on a pair of concentric tubes that are impedance matched to and co-axially aligned with the input bar and arranged to operate sequentially. The tandem momentum traps provide a single specimen loading event, of a predefined intensity and duration, without the need to initially offset the momentum traps from the input bar by accurate preset gaps. The method is relatively simple to set up and operate, which allows for routine specimen recovery during dynamic testing. The operation of the tandem momentum trap is demonstrated by an investigation of the dynamic mechanical properties of soft cancellous bovine bone specimens.

Keywords Cancellous bone · Momentum trap · Dynamic interrupted tests · Specimen recovery · Split Hopkinson pressure bar

Introduction

The design of protective structures to prevent injury during impact loading events, such as sporting accidents and vehicle collisions, requires a detailed understanding of the mechanisms of dynamic bone deformation and fracture. In particular, it is important to characterize cancellous bone under loading conditions similar to that encountered in daily life, so as to contribute to improved designs for protective equipment and preventive strategies that are better adapted to people and their activities.

The mechanical response of both cortical and cancellous bone has been widely studied. These studies have typically been conducted at either quasi-static or dynamic loading rates [1–3] with few studies incorporating the intermediate strain rate regime. Quasi-static cancellous bone studies have revealed strong links between the microstructure and the macroscopic mechanical response [4]. The localized fracture of cancellous bone at low strain rates has been shown to be strongly dependent on the heterogeneous porous architecture of the trabecular microstructure [5, 6]. To date, this work has only been conducted using interrupted quasi-static tests where specimens were compressed to predetermined strains. Technical challenges involved in conducting similar interrupted tests at higher strain rates have led to a lack of microstructural damage investigations of cancellous bone subjected to strain rates that are representative of those at which bone fracture events occur in daily life [7, 8].

The standard split Hopkinson pressure bar (SHPB) setup cannot be employed for interrupted testing due to stress wave reflections from the free ends that reload the specimen, leading to its compaction [9–11]. The removal of reflected compressive stress waves was first achieved by Nemat-Nasser et al. [12] using a momentum trap technique applied to a tensile split Hopkinson bar (TSHB). The momentum trap was in the form of a metal bar, with the same impedance as the input bar, aligned such that it was co-axial to the input bar and offset from the free end by a small gap. The gap was precision set such that the action of

✉ Trevor John Cloete
trevor.cloete@uct.ac.za

[1] LBM/Institut de Biomécanique Humaine Georges Charpak, Arts et Métiers ParisTech, 151 Boulevard de l'Hôpital, 75013 Paris, France

[2] Blast Impact and Survivability Research Unit (BISRU), Department of Mechanical Engineering, University of Cape Town (UCT), Private bag X3, Rondebosch 7701, South Africa

a tubular striker impacting upon a collar at the free end of the input bar would cause the gap to close but leave the bars just short of being in contact. Consequently, the reflected compressive wave returning from the specimen end of the input bar would immediately lead to contact with the momentum trap such that the entire compressive wave would be transferred into the momentum trap. Subsequent stress wave reflections in the momentum trap would cause it to separate from input bar, thus leaving the input bar quiescent and preventing further loading of the specimen. A similar system was developed by Lataillade et al. [13], which included a tubular momentum trap to capture the transmitted tensile wave at the free end of the transmitter bar.

A similar gap setting approach for the interrupted dynamic compressive testing of soft materials using an otherwise standard SHPB setup was reported by Song and Chen [14]. In this case, the momentum trap was replaced by a large reaction mass through which the input bar passed. The reaction mass was offset from a collar on the free end of the input bar by a small precision set gap. The action of a cylindrical striker impacting upon the free end of the input bar would cause the gap to close but leave the collar just short of being in contact with the reaction mass. The reflected tensile wave returning from the specimen end of the input bar would immediately lead to contact between the collar and the reaction mass. However, the reaction mass had an impedance that was several times larger than that of the input bar and essentially acted as a 'rigid' boundary. Consequently, the returning tensile wave would reflect off the reaction mass as another tensile wave and, upon reaching the specimen end, caused the input bar to separate from the specimen. In other words, the motion of the input bar would be reversed, thus unloading the specimen, even though the input bar was not left quiescent.

The aforementioned methods rely on an accurately preset gap between the momentum trap (or reaction mass) and a transfer flange at the impact end of the input bar. In addition, these methods require the impact speed of the striker to be accurately controlled, since any variation will affect the size of the residual gap after the striker rebounds. While the initial size of the required gap can be estimated theoretically, Nemat-Nasser et al. report that the final gap size and striker velocity must be optimized by trial and error [12]. Hence, these techniques can be time consuming and require a relatively highly level of operator skill and experience, which makes them inconvenient for routine testing by novice operators.

In this paper, an interrupted dynamic testing technique based on a tandem momentum trap (TMT) concept is presented. The technique does not require accurate gap setting and can be used routinely by a novice operator. This work represents an extension of a previously published feasibility study [15] where this technique was used to investigate the microstructure of recovered specimens. A recent variation of this technique was adapted to tensile testing by Isakov et al. [16], which has demonstrated the feasibility of this approach to different Hopkinson bar arrangements. The aim of this paper is to present a detailed development of the tandem momentum trap experimental technique as adapted for a Split Hopkinson Pressure Bar. To illustrate the technique, data from a small series of dynamic recovery experiments on cancellous bone are presented. This data forms a subset of that previously presented by Prot et al. [7, 15].

Experimental Technique

Operating Principle of a Tandem Momentum Trap

The operating principle of a tandem momentum trap, as adapted to a SHPB, is shown in Fig. 1. The striker, launched by a gas gun, impacts upon the flange threaded to the input bar. This results in two separate compressive waves, the first propagating through the input bar and the second through first momentum trap (Fig. 1b). The striker will rebound after the impact, provided that its impedance is less than the combined impedance of the input bar and the first momentum trap (Fig. 1c). Since both momentum traps are designed to be impedance matched with one another and the input bar, the second wave transfers to the second momentum trap without reflection (Fig. 1c). When the wave reaches the free end of the second momentum trap, it is reflected as a tensile wave (Fig. 1d). Upon reaching the interface with the first momentum trap, which cannot support a tensile load, the tensile wave reflects as a compressive wave and causes the separation of the second momentum trap from the first (Fig. 1e). Provided that the striker has the same wave speed but is shorter than the momentum traps, all the energy of the second stress wave will be captured in the second momentum trap while the first momentum trap will again be motionless and remain in contact with the flange. The ability for the first momentum trap to remain in contact with the first transfer flange is what distinguished the tandem momentum trap technique from previous techniques [12, 13].

Meanwhile, in accordance with a standard SHPB, the first compressive wave in the input bar propagates until the interface with the specimen. There, the wave is partially

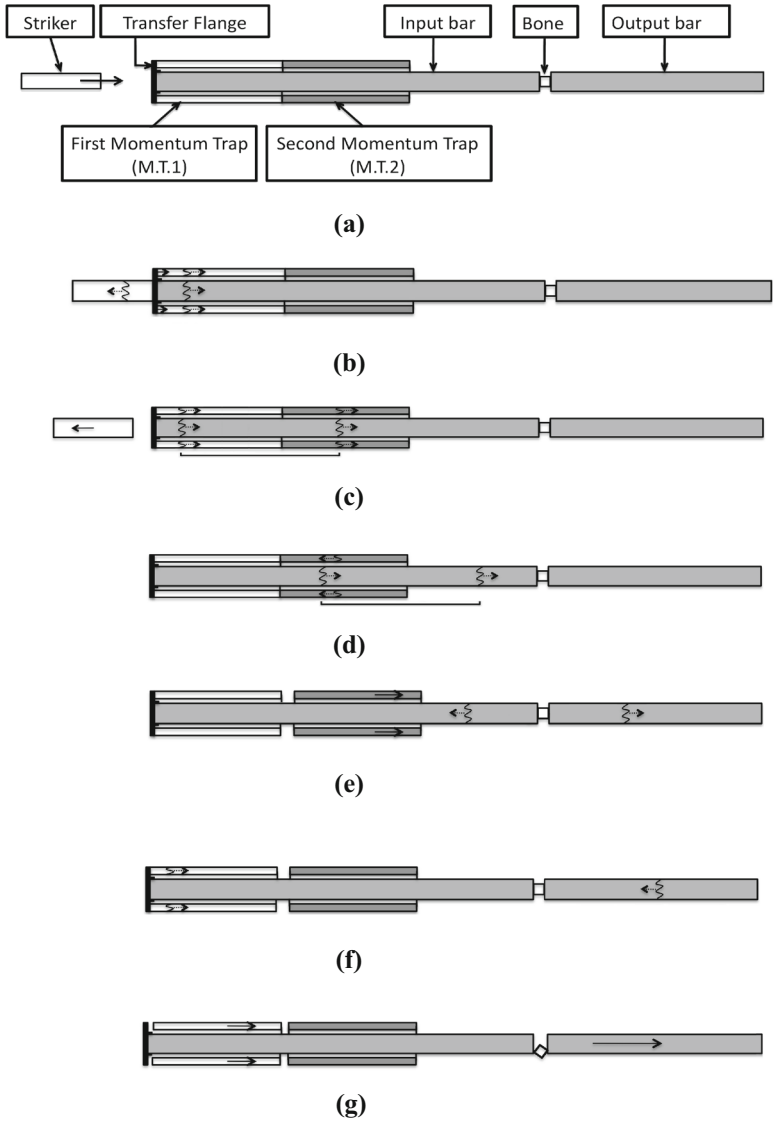

Fig. 1 Schematic illustration of the operating principle of a standard SHPB with a tandem momentum trap. **a** Initial configuration of a standard SHPB with a tandem momentum trap. **b** Propagation of the compression waves through striker and both the input bar and momentum trap 1. **c** Rebound separation of the striker with transfer of the compression wave through momentum trap 1 into momentum trap 2, while the compressive wave in the input bar propagates towards the specimen. **d** Reflection of the compression wave at the free end of momentum trap 2. **e** Separation of momentum trap 2 from momentum trap 1, which is left in contact with the collar, while stress wave interactions at the specimen interfaces create a reflected tensile pulse in the input bar and a compressive transmitted pulse in the output bar. **f** Complete transmission of the reflected tensile pulse into momentum trap 1, which leaves the input bar quiescent, while a reflected tensile wave propagates in the *output bar*. **g** Separation of momentum trap 1 from the input bar, along with separation of the *output bar*, which leads to recovery of the specimen after a single loading event

reflected back into the input bar as a tensile wave while the remainder is transmitted through specimen and into the output bar (Fig. 1e). The transmitted wave is reflected as a tensile wave at the end of the output bar and propagates back toward to the specimen interface (Fig. 1f) where it causes the output bar to separate from the specimen (Fig. 1g). In a similar way, the reflected tensile wave in the input bar, upon reaching the flange at the impact end, is transferred to the first momentum trap as a compressive wave which subsequently causes the separation of the first momentum trap (Fig. 1g). In this way no further stress wave reflections occur in the input bar. Consequently, the specimen experiences on a single load of known amplitude and duration.

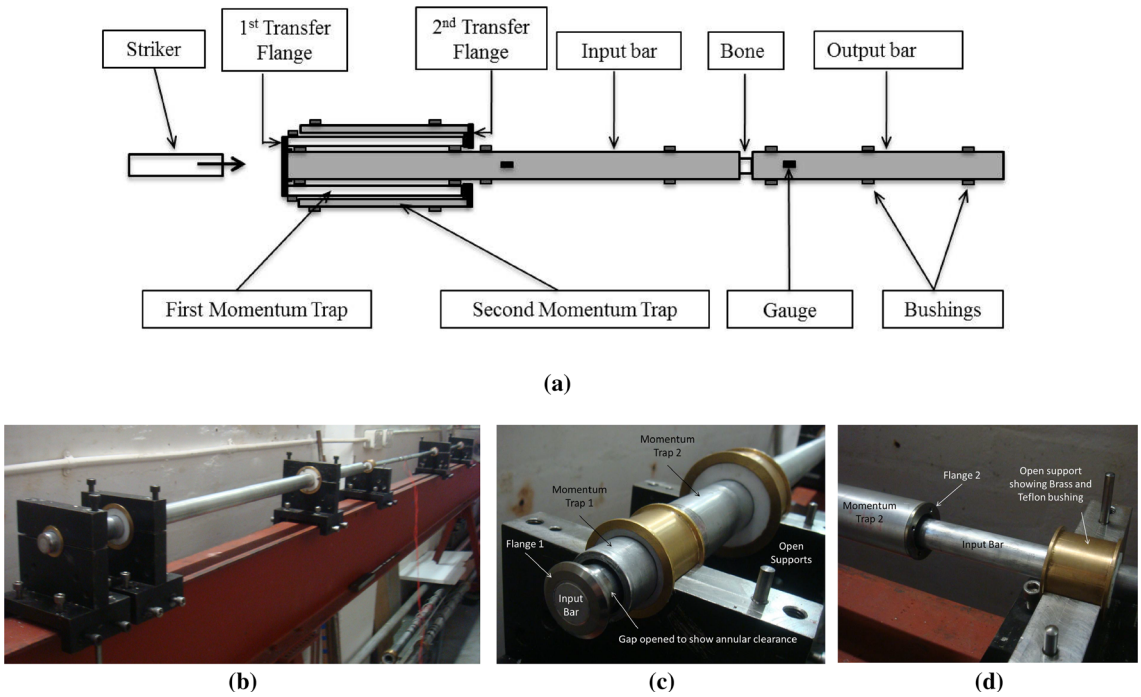

Fig. 2 Schematic diagram and detailed photographs of the practical implementation of a tandem momentum trap configuration for an otherwise standard SHPB

Unlike the momentum trapping concepts reviewed in the introductory section, the tandem momentum trap concept does not require any small accurate preset gaps between the input bar flange and momentum traps. Consequently, this approach will not be sensitive to small variations in the impact speed of the striker and will not require optimization by trial and error [12]. Therefore, tandem momentum trapping technique is suitable for routine testing by novice operators.

Practical Configuration of the Tandem Momentum trap for a SHPB

In a standard SHPB, the strain gauges are mounted at the middle of the input bar in order to separate the incident and the reflected waves, which requires a change in the momentum trap configuration from that discussed in the preceding section. The final configuration is shown in Fig. 2, where the tandem momentum traps are arranged as nested concentric impedance matched tubes, with the first momentum trap aligned with the input bar within the second momentum trap. The stress waves are transferred between the momentum traps through a second flange threaded to the second momentum trap.

For the tests reported in this paper, the input bar was made from 7075-T6 aluminium, while the output bar was made from magnesium to increase the sensitivity of the output signal. The dimensions and properties of the bars are given in Table 1. The momentum traps were made from standard size 6064-T6 aluminium tubing, where the inner tube diameters were chosen to be as close as possible to the outer diameter of the inner nesting parts, while the outer tube diameters were machined such that the tubes had the same cross-sectional area as the input bar to satisfy the impedance matching requirement. The lengths of the

Table 1 SPHB and momentum trap component specifications

	Input bar	Output bar	Momentum trap 1	Momentum trap 2	Strikers
Material	Aluminium	Magnesium	Aluminium	Aluminium	Aluminium
Length (mm)	3662	1998	1400	1350	250, 500, 750
Inner diameter (mm)	–	–	23	31.6	–
Outside diameter (mm)	19.1	19.8	30.1	36.9	19.1
Impedance (kPa.s/m)	13,941	9089	13,941	13,941	13,941
Density (g/cm^3)	2.77	1.82	2.77	2.77	2.77

momentum traps were chosen to be as long as possible without interfering with the strain gauges bonded to the input bar. The momentum trap and striker properties are also given in Table 1. Finally, the two flanges were made from Titanium (Ti-6Al-4V) to obtain strength and stiffness, while keeping the mass low.

As indicated in Fig. 2a, the output bar was supported by three Teflon bushings. Similarly, the midsection and specimen end of the input bar were supported by Teflon bushings, while the impact end of the input bar had to be indirectly supported due the presence of the first momentum trap. In this case the impact end of the first momentum trap was supported in an external Teflon bushing, while the input bar was, in turn, supported by a Teflon bushing pressed into the first momentum trap. A similar arrangement was used at the other end of the first momentum trap, although, in this case, the bar provided support for the first momentum trap. The annular clearance between the input bar and first momentum trap was 1.6 mm, which was dictated by the available standard aluminum tube sizes. This relatively large clearance resulted in the transfer flanges being more compliant that intended, which led to suboptimal behavior of the TMT concept, as will be discussed in Sect. 3. In contrast to the mutually supportive arrangement of the input bar and first momentum trap, the second momentum trap was independently mounted in two external Teflon bushings and only made contact with the first momentum trap through the second transfer flange. The annular clearance between the first and second momentum traps was 0.75 mm, which, as before, was dictated by the available standard aluminum tube sizes.

Provided that the striker is shorter than the momentum traps so as to allow for the complete momentum trapping of the reflected stress pulse, the striker length can be chosen to satisfy other test parameters, such as a specified final strain. For a cancellous bone specimen, which is relative soft in comparison to the Hopkinson bar materials, the deformation can be assumed to be dominated by the input bar. Hence, using standard elastic stress wave theory [17], the required specimen strain rate $\dot{\varepsilon}$ can be estimated for a specified interrupting strain ε_{int} and test duration Δt, which is the time for an elastic stress wave to traverse twice the length of the striker. In other words,

$$\dot{\varepsilon} = \frac{\varepsilon_{\text{int}}}{\Delta t} = \frac{C_s \varepsilon_{\text{int}}}{2L_s}, \tag{1}$$

where C_s and L_s are, respectively, the elastic wave speed and length of the striker.

Consequently, using co-linear elastic impact theory [17] and assuming uniform specimen deformation, the required striker impact velocity v_0 is,

$$v_0 = \frac{A_s + A_b + A_{MT1}}{A_s}\left(\frac{1}{2}\dot{\varepsilon}L_{spec}\right) = \frac{3}{2}\dot{\varepsilon}L_{spec}, \tag{2}$$

where A_s, A_b and A_{MT1} are the respective cross-sectional areas of the striker, input bar and first momentum trap, while L_{spec} is the specimen length. Note that the inclusion of the A_{MT1} term is required because the striker interacts with both the input bar and momentum trap during impact, while that factor of ½ accounts for the bar end velocity being twice that of the stress wave particle velocity.

For the experiments reported in this paper, the striker, input bar and momentum traps all had the same cross-sectional area, which leads to the final expression in Eq. 2. For specimens with large impedance values relative to the Hopkinson bars, such as cortical bone, the hardening of the specimen during a dynamic test needs to be accounted for, especially if a constant strain rate is required. This can be accomplished using pulse shaping techniques and their associated simple one dimensional numerical models [18]. Finally, the preceding analysis also serves to highlight two limitations of the TMT technique. Firstly, for a given final strain, a series of strikers of differing lengths are required to cover a range of strain rates and, secondly, for a given strain rate, a higher impact velocity is required in comparison to a standard SHB, which limits the upper strain rate range.

Commissioning and Material Testing

Several preliminary tests were conducted to determine the influence of various design features, such as the flange configuration and material choices. For example, three distinct flange materials were investigated, namely Titanium (Ti), high-density polyethylene (HDPE) and Aluminium (Al, identical to the bar material). A test was conducted in which the input bar was reversed such that the striker impacted upon the non-threaded end and the threaded collar was placed in contact with an Aluminium tube. The test results showed that, the Ti flange, which was the heaviest and stiffest of the three, performed the best. This suggests that the flange stiffness, rather than the mass or material dissimilarity, is of primary concern. Hence, Ti was chosen as the flange material. In addition, Ti has the benefit of being a strong, corrosion resistant and dissimilar to Al, which help prevent binding of the flange to the threaded bar and tube. Furthermore, conventional dynamic calibration tests were performed on the input bar with the flange attached but the output bar and momentum trap omitted. These results were compared to calibration tests without the flange attached, which showed that effect of flange mass was insignificant. The majority of the

commissioning tests produced similar expected results. Hence, for the sake of brevity, only the final tandem momentum trap commissioning tests will be reported in detail in Sect. 3.

Following the commissioning tests, 21 cancellous bovine bone specimens were machined for quasi-static or dynamic compression. Cylindrical specimens (diameter: 10 mm, length: 10 mm) were extracted from fresh bovine femoral bones (4 years old cattle). Hydrated specimens were then preserved in separate containers in a frozen condition. Before testing, the specimens were slowly thawed for 12 h at 5 °C and then exposed to room temperature (approximately 24 °C) prior to mechanical testing. Typical experimental results will be presented to show the effectiveness of the tandem momentum trap.

Results and Discussion

Tandem Momentum Trap Efficiency

A typical result for testing the input bar with the tandem momentum trap arrangement in place, but without the output bar or specimen, is shown in Fig. 3. In this configuration, an ideal momentum trapping system would result in approximately rectangular incident and reflected pulses, with essentially flat plateau regions, followed by no further significant stress wave oscillations.

Figure 3 shows the result of a test where no pulse smoothing was applied. It is evident that voltage peaks occur at the beginning and end of the plateau regions. This non-ideal behaviour appears to be due to the compliance of the flange connection. Upon application of a load, a finite amount of deformation is required before the flange connection can bear the full load. This deformation takes a finite time and hence the initial portion of the stress wave is not transferred to the first momentum trap, i.e. a greater proportion of the impulse is transferred to the input bar which results in the first signal peak (Peak 1). However, this effect has a short duration and as the flange connection stiffens a greater portion of the impulse is transfer to the first momentum trap, while that transferred to the input bar rapidly asymptotes to the expected value. The second peak (Peak 2) is essentially the reverse of the first peak, i.e. it is a result of the unloading of the flange connection. Similar signal peaks are evident in the results of Isakov et al. [16] who, on the basis of numerical simulations, presents an alternative 'hit and stick' effect due to a fillet feature of their flange connection design.

After the incident and reflected waves, another two peaks occurred, which are highlighted in Fig. 3. High speed camera footage suggests that the third peak (Peak 3) is to be due to a small gap that develops between the flange and the first momentum trap due to incomplete momentum transfer from the first momentum trap to the second as a result of compliance in the second flange connection. This gap causes the initial portion of the returning tensile wave to reflect back into the input bar until the gap closes and the rest of the tensile wave is trapped. This interpretation implies that a shorter striker with the same impact velocity should cause similar first and second peaks, but a smaller third peak, and was confirmed experimentally as shown in Fig. 4.

Lastly, a lower fourth peak is evident in Fig. 3. This peak cannot be due to the aforementioned gap since at this stage it is closed. Similar minor oscillations were observed to remain in the input bar by Isakov et al. [16], who argued

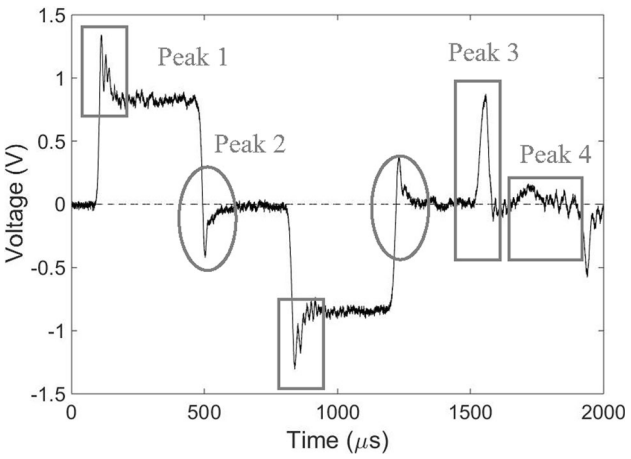

Fig. 3 *Input bar* signals from tandem momentum trap commissioning tests without pulse smoothing, where the specimen and *output bar* were omitted

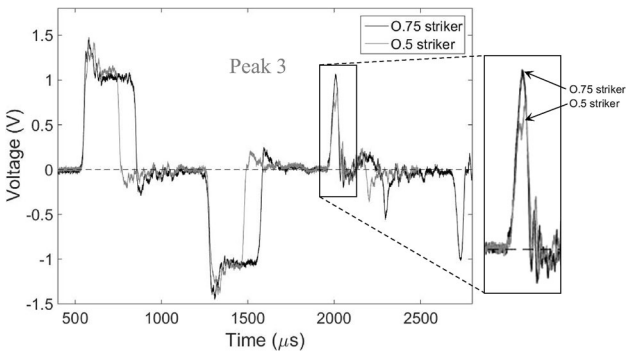

Fig. 4 Comparison of the effect of the striker length on the non-ideal signal peaks

that they are due to non-perfect alignment of the tubes and bars.

Despite these imperfections, the majority of the reflected wave is captured by the momentum traps. Furthermore, the residual pulses merely caused the end of the input bar to oscillate about a mean position with an amplitude of, at most, 3 % of the total displacement. In other words they led to no significant subsequent deformation of the specimen.

Interrupted High Strain Rate Testing of Cancellous Bone

A series of experiments were conducted to investigate the response of bovine cancellous bone to different combinations of dynamic loading. Equilibrium across the specimen interfaces was assessed by comparing interface stress history obtained from the input and output bars. A typical example is shown in Fig. 5, which confirms that equilibrium had been achieved, with no significant delay in the ring-up time.

The tandem momentum traps allowed interrupted experiments to be conducted such that intact specimens were recovered with final strain values varying from 5 to 16 %, as shown in Table 2 and Fig. 6. In particular, this technique allows for tests to be interrupted at strains that are associated with the plateau stress but before densification of the broken trabeculae. The measured interrupted strains are mostly in accordance with the predicted values obtained using Eq. 1, as shown in Table 2. Figure 6 shows that the observed ultimate stress values for this study ranges from 8 to 60 MPa. This amount of scatter is typical of cancellous bone [19] and is not due to the tandem momentum trap concept.

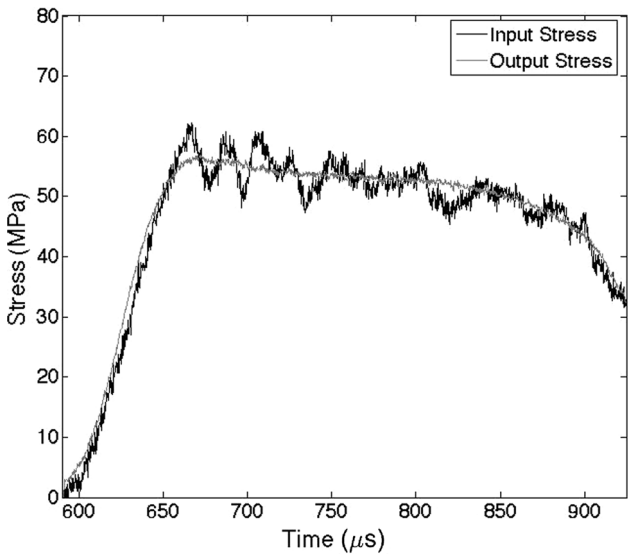

Fig. 5 Equilibrium across the interfaces of a cancellous bone specimen

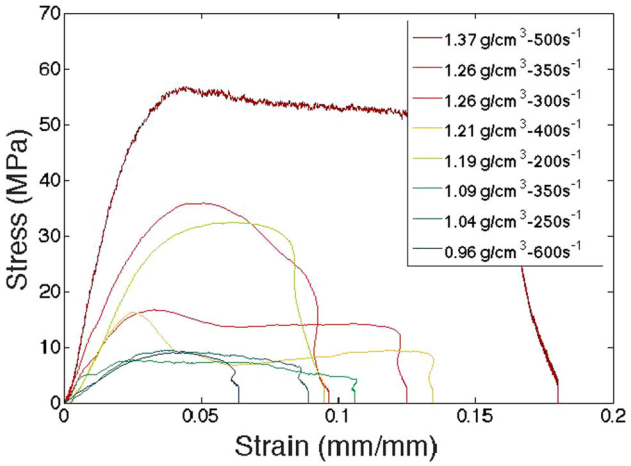

Fig. 6 Test results for cancellous bone subjected to interrupted dynamic compression

High speed camera data was used to confirm that the specimens were only subjected to a single loading event, as shown in Fig. 7. In particular, it is evident that, after the loading of the specimen, the face of the input bar does not advance any further, while the output bar, which does not have a momentum trap moves away. Furthermore, Fig. 7 shows the timing of the camera images relative to the strain gauge signals from the input and output bars. In addition, a portion of the output signal is shown transposed to the specimen interface such that the timing of the images relative to the specimen loading history is evident.

Finally, an example of the data that can be obtained using the TMT technique is shown in Fig. 8, where the sensitivity of the apparent Young's modulus of bovine cancellous bone to strain rate is shown as a function of the apparent specimen density. It is evident that there is a large amount of intrinsic scatter in the data, but there nevertheless appears to be a distinct strain rate effect.

Table 2 Predicted (Eq. 1) and measured interrupted strains

Striker length (m)	0.75	0.75	0.75	0.5	0.75	0.75	0.5	0.75	0.25
Measured Strain rate (/s)	350	350	400	300	250	200	200	500	600
Measured interrupted strain (%)	11	12	13	8	9	7	9	16	5
Predicted interrupted strain (%)	10	10	12	6	8	6	4	15	3

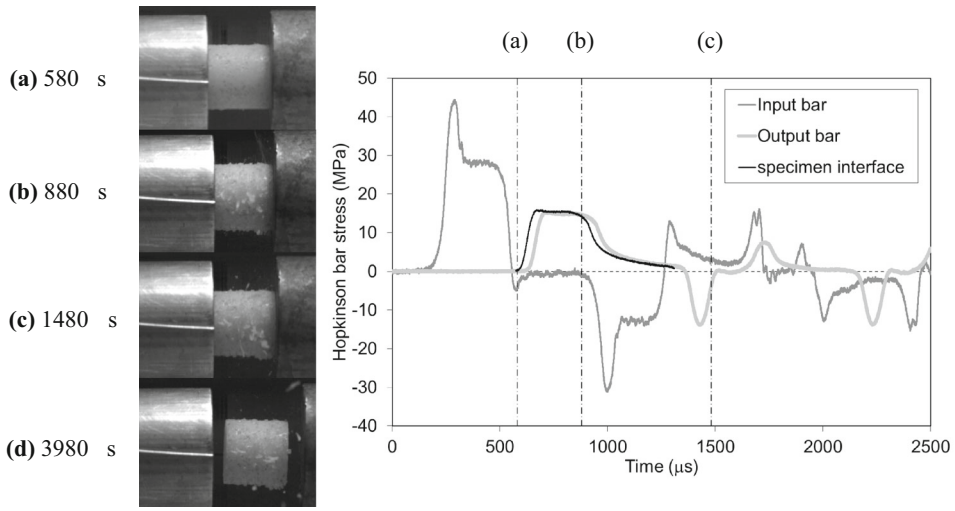

Fig. 7 High speed camera footage of an interrupted dynamic compression of a cancellous bone specimen

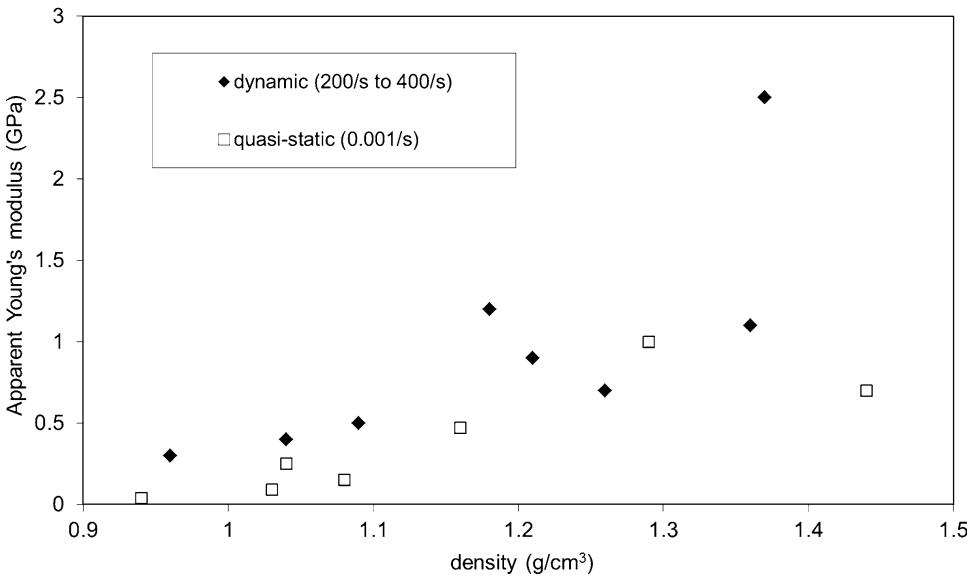

Fig. 8 Comparison of the sensitivity of the apparent Young's modulus of bovine cancellous bone to variations of apparent specimen density and strain rate

Conclusions

A new dynamic specimen recovery technique based on a tandem momentum trap concept, as applied to an otherwise standard split Hopkinson pressure bar, has been presented. The technique allows for routine dynamic specimen recovery without the need for accurate gap presetting and thus improves the ease and repeatability of the test. Notwithstanding some sub-optimal performance, the effectiveness of the tandem momentum trap technique was validated by the successful dynamic recovery of cancellous bone specimens after a single deformation event of known amplitude and duration.

Acknowledgments The authors wish to thank Mr. G. Newins and Mr. C. Nicholas from the mechanical workshop of the Mechanical Engineering Department of the University of Cape Town for machining the apparatus. The authors wish also to thank Dr Steeve Chung Kim Yuen for his assistance with the high speed camera footage.

References

1. Johnson T, Socrate S, Boyce M (2010) A viscoelastic, viscoplastic model of cortical bone valid at low and high strain rates. Acta Biomater 6:4073–4080. doi:10.1016/j.actbio.2010.04.017
2. Kefalas V, Eftaxiopoulos DA (2012) Experimental study of cancellous bone under large strains and a constitutive probabilistic model. J Mech Behav Biomed Mater 6:41–52. doi:10.1016/j.jmbbm.2011.10.006
3. Teja CK, Chawla A, Mukherjee S (2012) Determining the strain rate dependence of cortical and cancellous bones of human tibia using a Split Hopkinson pressure bar. Int J Crashworthiness. doi:10.1080/13588265.2012.730212
4. Follet H, Viguet-Carrin S, Burt-Pichat B, Dépalle B, Bala Y, Gineyts E, Munoz F, Arlot M, Boivin G, Chapurlat RD, Delmas PD, Bouxsein ML (2011) Effects of preexisting microdamage, collagen

cross-links, degree of mineralization, age, and architecture on compressive mechanical properties of elderly human vertebral trabecular bone. J Orthop Res 29(4):481–488. doi:10.1002/jor.21275
5. Tassani S, Matsopoulos GK (2014) The micro-structure of bone trabecular fracture: an inter-site study. Bone 60:78–86. doi:10.1016/j.bone.2013.12.007
6. Hernandez CJ, Lambers FM, Widjaja J, Chapa C, Rimnac CM (2014) Quantitative relationships between microdamage and cancellous bone strength and stiffness. Bone 66:205–213. doi:10.1016/j.bone.2014.05.023
7. Prot M, Saletti D, Pattofatto S, Bousson V, Laporte S (2015) Links between mechanical behavior of cancellous bone and its microstructural properties under dynamic loading. J Biomech 48(3):498–503. doi:10.1016/j.jbiomech.2014.12.002
8. Hansen U, Zioupos P, Simpson R, Currey JD, Hynd D (2008) The effect of strain rate on the mechanical properties of human cortical bone. J Biomech Eng 130(1):011011. doi:10.1115/1.2838032
9. Shim VPW, Yang LM, Liu JF, Lee VS (2005) Characterisation of the dynamic compressive mechanical properties of cancellous bone from the human cervical spine. Int J Impact Eng 32(1):525–540. doi:10.1016/j.ijimpeng.2005.03.006
10. Pilcher A, Wang X, Kaltz Z, Garrison JG, Niebur GL, Mason J, Chen W (2010) High strain rate testing of bovine trabecular bone. J Biomech Eng 132(8):081012. doi:10.1115/1.4000086
11. Teja CK, Chawla A, Mukherjee S (2013) Determining the strain rate dependence of cortical and cancellous bones of human tibia using a Split Hopkinson pressure bar. Int J Crashworthiness 18(1):11–18. doi:10.1080/13588265.2012.730212
12. Nemat-Nasser S, Isaacs JB, Starrett JE (1991) Hopkinson techniques for dynamic recovery experiments. Philos T Roy Soc A 435(1894):371–391. doi:10.1098/rsta.1991.0150
13. Lataillade JL, Delaet M, Collombet F, Wolff C (1996) Effects of the intralaminar shear loading rate on the damage of multi-ply composites. Int J Impact Eng 18(6):679–699. doi:10.1016/0734-743X(95)00059-J
14. Song B, Chen W (2005) Split Hopkinson pressure bar techniques for characterizing soft materials. Latin Am J Solids Stru 2(2):113–152
15. Prot M, Cloete TJ, Pattofatto S (2012) Dynamic compression and recovery of cancellous bone for microstructural investigation. EPJ Web of Conferences 26:03003. doi:10.1051/epjconf/20122603003
16. Isakov M, Hiermaier S, Kuokkala VT (2014) Improved specimen recovery in tensile split Hopkinson bar. Philos T Roy Soc A 372(2023):20130194. doi:10.1098/rsta.2013.0194
17. Spotts MF (1964) Mechanical design analysis. Prentice-Hall, Upper Saddle River
18. Cloete TJ, van der Westhuizen A, Kok S, Nurick GN (2009) A tapered striker pulse shaping technique for uniform strain rate dynamic compression of bovine bone. In: DYMAT-2009, EDP Sciences, pp 901–907. doi: 10.1051/dymat/2009126
19. Yeni YN, Hou FJ, Vashishth D, Fyhrie DP (2001) Trabecular shear stress in human vertebral cancellous bone: intra-and inter-individual variations. J Biomech 34(10):1341–1346. doi:10.1016/S0021-9290(01)00089-6